Trans-critical vapor compression cycle using butane (R600) as refrigerant for industrial waste heat recovery

Manuel VERDNIK, René RIEBERER, Heinz MOISI

Institute of Thermal Engineering, Graz University of Technology
Graz, 8010, Austria, manuel.verdnik@tugraz.at

ABSTRACT

By utilizing a trans-critical vapor compression cycle using hydrocarbons, the operating range of these natural refrigerants with low global warming potential and zero ozone depletion potential can be extended to higher temperature levels.

A single-stage cycle using a reciprocating (suction gas cooled) compressor and an internal heat exchanger for suction gas superheating has been modeled using Modelica and the TIL thermal component library. The simulation model has been validated by means of experimental data gathered with a R600 test rig operated at condensing temperatures up to 110°C.

The simulation model was modified to study the system behavior in trans-critical operation. Increasing the suction gas superheat lowers the values for the high-side pressure at which the maximum efficiency is reached, which could be utilized if the high-side pressure is limited by the used components. Through the application of an internal heat exchanger, the increase of superheat shows potential to increase the Coefficient of Performance (COP).

Keywords: Heat Recovery, High Temperature, Hydrocarbon, Trans-critical Cycle.

1. INTRODUCTION

With an energy consumption of 148 EJ, the industrial sector accounted for 37% of the world's total final energy consumption in 2016 (IEA, 2018). Recovering waste heat through the utilization of high temperature heat pumps can increase process efficiencies and decrease the use of fossil fuels, thus leading to a reduction in CO_2 emissions. In order to reduce the greenhouse gas emissions caused by the release of refrigerants to the atmosphere, the Kigali amendment to the Montreal protocol regulates a step-wise phase down of refrigerants with a high global warming potential (UNEP, 2016). Currently, heat supply temperatures up to 160°C are achievable with vapor compression heat pumps using the refrigerant R1336mzz-Z in the Viking Heat Booster (Viking, 2018). The Kobe Steel SGH 165 produces steam at 120 °C with a R245fa vapor compression heat pump and compresses it further to 165 °C (Arpagaus et al., 2018). Trans-critical vapor compression cycles allow an extension of the operating range of refrigerants beyond their critical temperature (Angelino and Invernizzi, 1994). Implemented with R744 (Lorentzen, 1990), this is a well-known technology (Austin and Sumathy, 2011), yet the application of other refrigerants is very limited. Besbes et al. (2015) developed a trans-critical R32 heat pump with a heat source temperature of 50°C and a heat sink temperature of 120°C.

The hydraulic layout and the t/h-diagram of a single-stage trans-critical vapor compression heat pump with an internal heat exchanger (IHX), using R600 as refrigerant is depicted in Fig. 1. After the compression to a high-side pressure exceeding the critical pressure of the refrigerant (37,96 bar), the heat rejection occurs at gliding temperature instead of condensation at constant temperature, as can be seen in the t/h-diagram in Fig. 1 (right). Without the relation between temperature and saturation pressure the necessary control of the high-side pressure can be obtained by adjusting the refrigerant mass in the according part of the cycle (Kim et al. 2004). In the observed cycle, this is realized with the pressure control valve (PCV) (Pos. 3). While the heat sink and source temperatures are boundary conditions set by the application, the suction gas superheat and the high-side pressure

can be adjusted to optimize the operation of the heat pump. To study the influence of these parameters, a simulation study based on a sub-critical test rig was carried out.

The sub-critical single-stage compression cycle equipped with a high-pressure receiver is modeled and validated with experimental data from a test rig, obtained by Moisi and Rieberer (2018). By adding a pressure control valve (PCV) at the receiver inlet (Pos. 3) as illustrated in Fig. 1, the high-side pressure can be raised above the critical pressure of the refrigerant, representing a trans-critical cycle with a medium pressure receiver. The test rig as well as the evaluation of the experimental data is described in Section 2, the simulation model is outlined in Section 3 and the results are presented in Section 4.
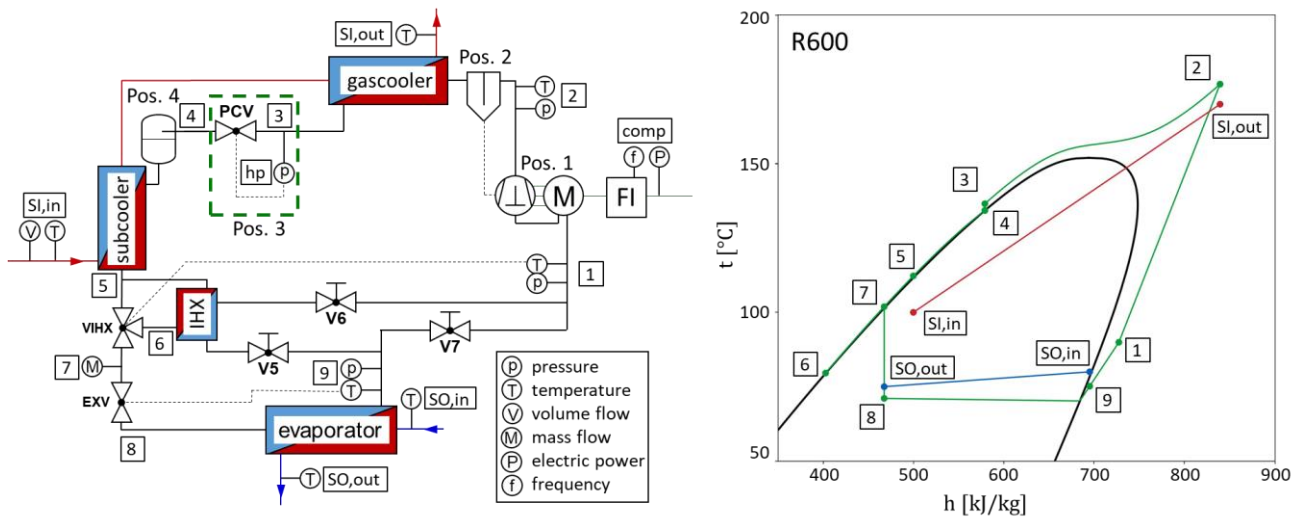

Figure 1: Hydraulic layout (left) and t/h-Diagram (right) of the studied trans-critical cycle

2. SUB-CRITICAL TEST RIG

The test rig of a sub-critical one-stage R600 high temperature heat pump has been developed during a preceding project (Moisi et al, 2018). The heat pump has a capacity of 45 kW at a heat source inlet/outlet temperature of 70/65 °C, a heat sink inlet/outlet temperature of 80/110 °C and an inverter frequency of 75 Hz (Moisi et al., 2017). The hydraulic layout depicted in Fig. 1 (left) corresponds to the refrigerant cycle of the sub-critical heat pump with the exception of the PCV. The suction gas superheating in the IHX can be adjusted with the 3-way-valve (VIHX). The IHX can be bypassed by closing the valves V5 and V6. A modified 30L-DLRX-13 separating hood reciprocating compressor (Pos. 1) from the project partner Frigopol equipped with a frequency inverter is used in the test rig. The modification of the compressor comprises a specially designed suction gas motor cooler to enable the necessary suction gas superheat needed to avoid wet compression due to an "overhanging" two-phase region of R600 (Moisi and Rieberer, 2016). To avoid accumulation of compressor lubricant in the refrigerant cycle, an oil separator (Pos. 2) is placed after the compressor. In sub-critical operation, the gascooler acts as condenser. The high-pressure receiver (Pos. 4) ensures saturated liquid state at the inlet of the subcooler. The electric expansion valve (EXV) regulates the refrigerant mass flow into the evaporator, thus controlling the suction gas superheat at the evaporator outlet. Brazed plate heat exchangers are used for the condenser, subcooler and evaporator. Water at a pressure of 2,5 bar is used in the heat sink and heat source cycles.

2.1. Measured Compressor and system efficiencies

Measurement data of the heat pump prototype at different operating points with an inverter frequency of 50 Hz, obtained by Moisi and Rieberer (2018), was used to evaluate the compressor and the system efficiencies. The positions of the sensors are depicted in Fig. 1. Relevant properties of R600 and water are obtained from the property database included in the software EES (2018). The overall isentropic efficiency, the internal isentropic efficiency and the volumetric efficiency of the compressor are calculated according to Eq. (1), Eq. (2) and Eq. (3) respectively.

$$\eta_{is,ov} = \frac{\dot{m}_{ref} \cdot (h_{ref,2s} - h_{ref,1})}{P_{el,comp}} \qquad \text{Eq. (1)}$$

$$\eta_{is,i} = \frac{h_{ref,2s} - h_{ref,1}}{h_{ref,2} - h_{ref,1}} \qquad \text{Eq. (2)}$$

$$\lambda_{vol} = \frac{\dot{m}_{ref}}{\rho_{ref,1} \cdot \dot{V}_{swept}} \qquad \text{Eq. (3)}$$

The dependency of the compressor efficiencies on the pressure ratio is expressed by polynomials using the least squares approximation. Measured efficiencies as well as the approximations are depicted in Fig. 2.
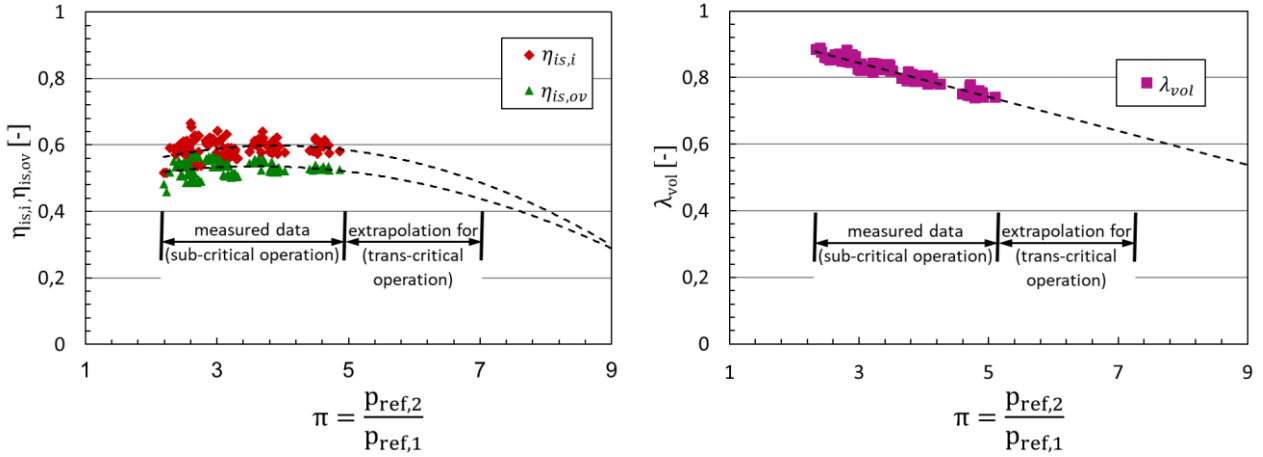

Figure 2: Overall isentropic and internal isentropic efficiency (left) and volumetric efficiency (right) of the Frigopol prototype compressor

The COP was evaluated with the measured heat release to the water cycle according to Eq. (4)

$$COP = \frac{\dot{Q}_{h,w}}{P_{el,comp}} = \frac{\dot{V}_{SI,in} \cdot \rho_{SI,in} \cdot cp_{SI,in} \cdot (t_{SI,out} - t_{SI,in})}{P_{el,comp}} \qquad \text{Eq. (4)}$$

3. SIMULATION MODEL

The TIL Suite package (TLK-Thermo, 2018), containing model libraries for components and media properties in the object-based Modelica language, was used to develop the simulation model for this study. Predefined models of the package can be extended with user specific geometries or correlations for heat transfer and pressure drop.

First, the sub-critical test rig was modelled without the PCV according to the hydraulic layout in Fig. 1 with exception to the neglected oil separator. For the trans-critical operation, the PCV was added. The following sections describe the modelling of the compressor and the heat exchangers.

3.1. Compressor

The compressor was modelled using the "efficiency based compressor model" included in TIL with efficiencies according to Eqs. (1) to (3) deduced from measurement data as described in section 2.1 for the prototype compressor from Frigopol. In order to investigate a different compressor, data for a Bitzer 4VE-10P operated with R134a were retrieved from the manufacturer's design software (Bitzer, 2018) to evaluate the efficiencies according to Eq. (1) and Eq. (3). Since there is no data for the compressor discharge temperature available in the software, the internal isentropic efficiency was assumed. The obtained polynomials as well as the nominal volumetric flow rate are listed in Table 1.

Table 1. Data used for modelling the compressor

	Frigopol 30L-DLRX-13 mod.	Bitzer 4VE-10P
$\eta_{is,ov}$	$0{,}4239 + 0{,}0619\pi - 0{,}0085\pi^2$	$0{,}6845 - 0{,}002\pi - 0{,}0004\pi^2$
$\eta_{is,l}$	$0{,}4211 + 0{,}0906\pi - 0{,}0116\pi^2$	$0{,}7600 - 0{,}002\pi - 0{,}0004\pi^2$
λ_{vol}	$0{,}9982 - 0{,}0512\pi$	$0{,}9747 - 0{,}0372\pi$
$\dot{V}_{swept}$ @ 50Hz	$29{,}94 \text{ m}^3 \cdot \text{h}^{-1}$	$34{,}7 \text{ m}^3 \cdot \text{h}^{-1}$

3.2. Heat Exchangers

The brazed plate heat exchangers are modeled with a finite volume approach and a discretization of 10 cells each. Geometrical data of the heat exchangers is listed in Table 2, a sinusoidal chevron pattern with a pattern angle of 60° is assumed for all heat exchangers.

Table 2. Geometrical data of the used heat exchangers

	Evaporator	Gascooler	Subcooler	IHX
Number of plates (-)	40	40	14	30
Length (mm)	466	476	250	250
Width (mm)	111	113	112,8	112,8
Pattern amplitude (mm)	1,91	1,68	1,91	1,91
Wall thickness (mm)	0,4	0,3	0,4	0,4

The heat transfer coefficients for evaporating and superheated R600 were calculated according to Longo et al. (2015), for condensing R600 the correlation by Akers et al. (1959) was used. Heat transfer coefficients for trans-critical operation were calculated using the correlation by Forooghi and Hooman (2014). The pressure drop in trans-critical operation, the heat transfer coefficient and pressure drop for liquid R600 in the subcooler and IHX as well as for the water side of the heat exchangers were calculated according to Martin (2013). The pressure drop during evaporation and condensation were calculated according to Longo et al. (2010) and Longo et al. (2012), respectively. The pressure drop for superheated R600 in the IHX was calculated according to Martin (2013).

4. RESULTS

4.1. Validation of the Model at Sub-critical Conditions

The COP measured at sub-critical operating points listed in Table 3 is compared with results from the simulation model, in both cases without the IHX. As can be seen from Fig. 3 (right), the relative deviation between simulation and experiment is less than 7% for all operating points.

Table 3. Experimentally investigated operation points (Moisi and Rieberer, 2018)

$t_{SO,in}$	50				60			70		80
$t_{SO,out}$	45				55			65		75
$t_{SI,in}$	50	60	70	80	60	70	80	70	80	80
$t_{SI,out}$	80	90	100	110	90	100	110	100	110	110
COP_{meas}	4.68	3.91	3.38	2.91	4.88	4.11	3.50	5.14	4.26	4.85
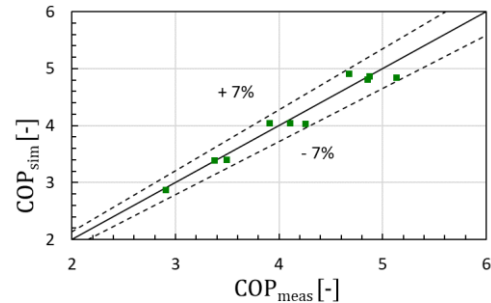
Figure 3. Comparison of simulated and measured COP at sub-critical conditions

4.2. Trans-critical Operation

Since the properties of a substance vary considerably in the vicinity of the critical point, the discretization of the gas cooler needs to be fine enough to consider these variations. In order to exclude the influence of the discretization of the gas cooler on the results of the simulation, the

variation of the COP with the high side pressure was investigated for different cell numbers in the gascooler. The value for the optimal high-side pressure at which the maximal COP occurs changed for simulations conducted with less than 80 cells. As more cells require more computational effort, especially during the initialization phase of the simulation, 80 cells were chosen as a tradeoff between computational effort and accuracy for the further simulations.

4.2.1. Optimal high-side pressure

At a fixed compressor inlet state, increasing the high-side pressure leads to an increase of the compressor outlet temperature (state point 2) and the required compressor power. Due to the heat rejection at gliding temperature in trans-critical operation and the curvature of a super-critical isobar, the location of the pinch point in the gascooler depends on the gas cooler inlet state and thus on the high-side pressure. At too low high-side pressures as depicted in Fig. 4 (left), the small temperature difference at the inlet of the gascooler affects the heat transfer, thus increasing the refrigerant temperature at the outlet of the gascooler (state point 3) and the subcooler (state point 5) and decreasing the heating capacity. Increasing the high-side pressure increases the temperature difference between refrigerant and heat sink medium at the inlet of the gascooler. This increases the heating capacity to the cost of increased compressor power. Fig. 4 (right) decipts a cycle with a too high high-side pressure. An optimum high-side pressure for achieving the highest COP at a certain operating point can be found as shown in Fig. 4 (middle).
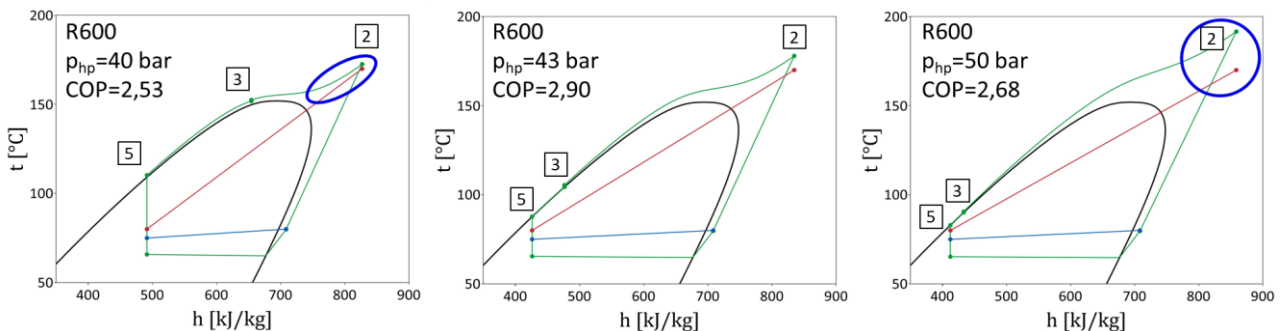

Figure 4: t/h-diagram for different high-side pressures at source inlet/outlet temperatures of 80/75 °C, sink inlet/outlet temperatures of 80/170 °C and a suction gas superheat of 15 K (without IHX)

4.2.2. Influence of the operating parameters

Simulation runs with different sink inlet temperatures but constant outlet temperature of 160 °C are shown in Fig. 5 (left). An increase in the sink inlet temperature leads to an increase of the refrigerant temperature at the subcooler outlet causing a decrease in the heating capacity (Moisi et al, 2018). Since the compressor power remains almost constant, a decline of the COP can be observed. The optimal value for the high-side pressure is not significantly influenced by the heat sink inlet temperature. Increasing the sink outlet temperature demands an increase of the high-side pressure. The increased compressor power leads to a drop of the maximal COP as can be seen in Fig. 5 (right).
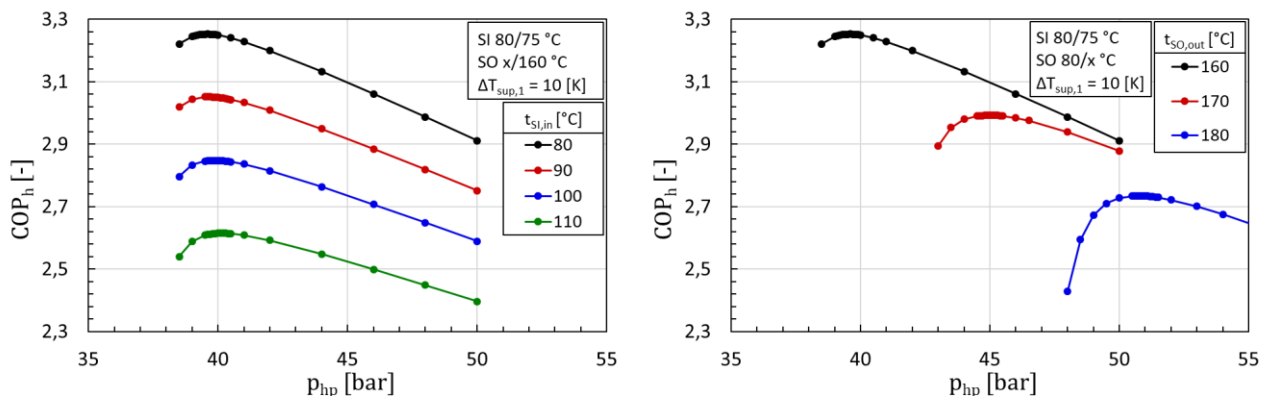

Figure 5: COP at varying sink inlet temperatures (left) and outlet temperatures (right) depending on the high-side pressure (without IHX)

The influence of a varying suction gas superheat realized in the evaporator (without using the IHX) can be observed in Fig. 6 (left). With increased superheat, the optimal high-side pressure drops. In cases where the maximum pressure is limited by components of the system, this can be used to reduce the necessary high-pressure level. However, as can be seen in Fig. 6 (right), the decreasing evaporation temperature at increasing superheat leads to a decrease in the heating capacity. The compressor power is almost constant because the decreased mass flow needs to be compressed at higher pressure differences. As a result, the COP decreases at increased superheat, which can clearly be seen in Fig. 6 (left).
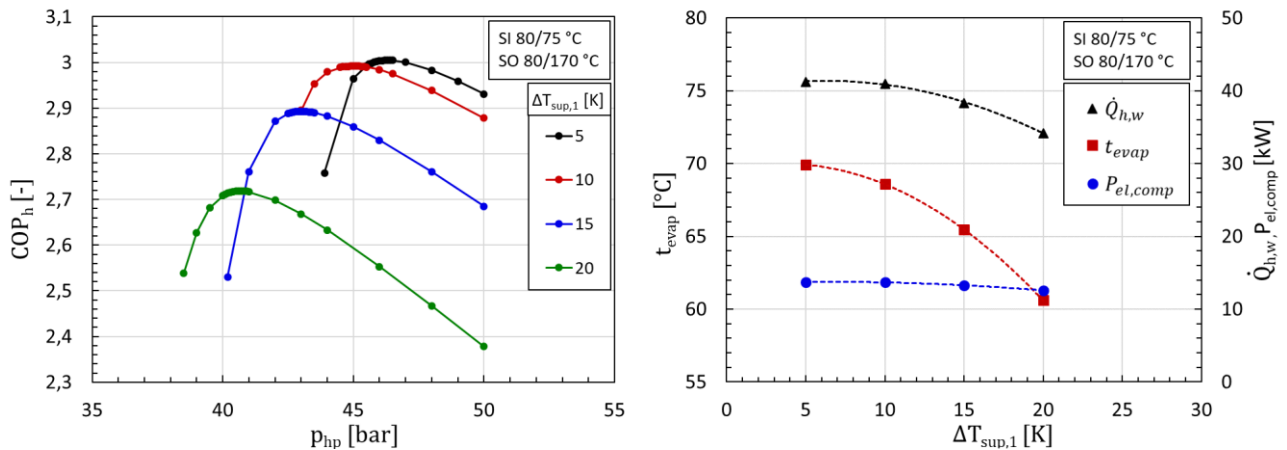

Figure 6: COP for different high-side pressures at varying suction gas superheat (left) and the influence of the superheat on evaporation temperature and capacities (right) (without IHX)

4.2.3. Possible improvements of the investigated cycle

The application of an internal heat exchanger as depicted in Fig. 1 enables an increase of the superheat without a decrease of the evaporation temperature. Fig. 7 (left) shows the COP at different values for suction gas superheat at the compressor inlet, where 5 K of superheat were obtained at the outlet of the evaporator and the rest was achieved using an IHX. As already observed without using the IHX, the optimal high-pressure drops but due to the IHX, the evaporation temperature does not decrease when increasing the suction gas superheat. As a result, the COP increases with increasing superheat because the compressor power remains almost constant while the heating capacity increases due to the increased superheat.

Another aspect for improvement is the used compressor. As can be seen from the efficiency data in Fig. 2, the prototype compressor is operated far outside the nominal operating range, thus leading to a deterioration of the efficiencies. Fig. 7 (right) shows the results with efficiency data for the Bitzer compressor as listed in Table 1. According to the simulation results, this compressor improves the COP and a further reduction of the optimal high-side pressure is possible.
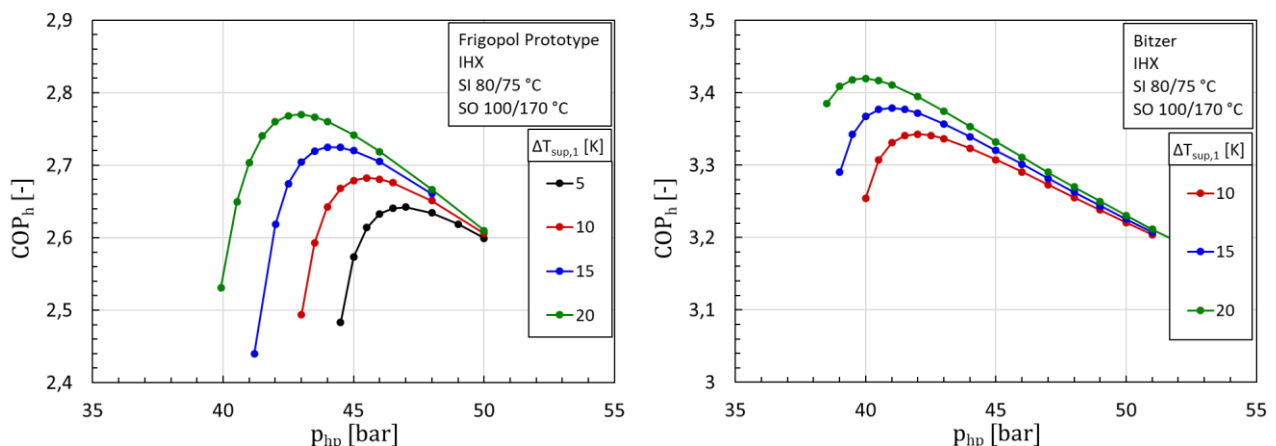

Figure 7: COP for different high-side pressures at varying suction gas superheat using an IHX with the Frigopol prototype compressor (left) and a Bitzer 4VE-10P (right)

5. CONCLUSIONS AND OUTLOOK

The introduced simulation model of a R600 high-temperature heat pump describes the COP of the sub-critical test rig with a deviation of less than 7% from the measured values.

By including a pressure control valve at the inlet of the receiver, trans-critical operation of the heat pump was investigated by means of simulation. The influence of the regulated high-side pressure on the COP showed an optimal value for each operating point that occurs at lower pressures if the suction gas superheat at the compressor inlet is increased. By using an internal heat exchanger, an increase of the COP by increasing the suction gas superheat is possible. At a heat source inlet/outlet temperature of 80/75 °C and a heat sink inlet/outlet temperature of 80/160 °C, the basic cycle without IHX using the Frigopol prototype compressor achieved a COP of 3.24 at a suction gas superheat of 5 K. At a sink inlet/outlet temperature of 100/170 °C, a COP of 2.64 was achieved. Using an IHX to raise the suction gas superheat to 20 K, the COP was improved to 2.77 while decrasing the high-side pressure from 47 to 43 bar. By using the Bitzer compressor, a further increase of the COP to 3.42 at a high-side pressure of 40 bar should be possible.

This study serves as the basis for the development of a prototype because application specific limitations of the components need to be taken into consideration. The model predicts compressor outlet temperatures 5-10 K higher than the sink outlet temperature at optimal high pressures, depending on the suction gas superheat. The expected high temperatures require special compressor lubricants such as Polyalphaolefin (PAO) oils. If suction gas cooled compressors are used, the maximum suction gas temperature represents a limit to the maximum evaporation temperature. The next steps will be to experimentally test the operating limits of the compressor such as the maximum high pressure and maximum suction gas temperature and then to develop a prototype for the trans-critical R600 vapor compression heat pump.

ACKNOWLEDGEMENTS

NOMENCLATURE

1…9	state point	$P_{el,comp}$	electric power of the compressor (kW)
COP	Coefficient of Performance	π	pressure ratio of the compressor (-)
cp	specific heat capacity (kJ·(kg·K)$^{-1}$)	$\dot{Q}_{h,w}$	heating capacity on water side (kW)
$\eta_{is,ov}$	overall isentropic efficiency (-)	ref	refrigerant
$\eta_{is,i}$	internal isentropic efficiency (-)	ρ	density (kg·m^{-3})
EXV	electric expansion valve	s	isentropic change of state
f	frequency (Hz)	SI	heat sink
h	specific enthalpy (kJ·kg^{-1})	sim	simulated
IHX	internal heat exchanger	SO	heat source
in	inlet	ΔT_{sup}	suction gas superheat (K)
λ_{vol}	volumetric efficiency	t	temperature (°C)
meas	measured	t_{evap}	evaporation temperature (°C)
$\dot{m}_{ref}$	refrigerant mass flow (kg·h^{-1})	V	valve
out	outlet	$\dot{V}$	volume flow
p	pressure (bar)	VIHX	3-way-valve internal heat exchanger
p_{hp}	high-side pressure (bar)	$\dot{V}_{swept}$	swept volume flow of the compressor (m^3·h^{-1})
PCV	pressure control valve		

REFERENCES

Akers, W.W., Deans, H.A., Crosser, O.K., 1959. Condensing heat transfer within horizontal tubes. Chemical Engineering Progress 54(10), 89-90

Angelino, G., Invernizzi, C., 1994. Supercritical heat pump cycles. International Journal of Refrigeration 17(8), 543-554

Arpagaus, C., Bless, F., Uhlmann, M., Schiffmann, J., Bertsch, S., 2018. High temperature heat pumps: Market overview, state of the art, research status, refrigerants, and application potentials. Energy 152, 985-1010

Austin, B., Sumathy, K., 2011. Transcritical carbon dioxide heat pump systems: A review. Renewable and Sustainable Energy Reviews 15(8), 4013-4029

Besbes, K., Youghaib, A., De Carlan, F., Peureux, J.-L., 2015. A R-23 transcritical heat pump for high temperature industrial applications. Proceedings of the IIR Conference of Refrigeration, Yokohama, Japan

Bitzer, 2018. Bitzer Software v. 6.9.2074, BITZER Kühlmaschinenbau GmbH, Sindelfingen, Germany

EES, 2018. Engineering Equation Solver v. 10.439, F-Chart Software, Madison, Wisconsin.

Forooghi, P., Hooman, K., 2014. Experimental analysis of heat transfer of supercritical fluids in plate heat exchangers. International Journal of Heat and Mass Transfer 74, 448-459

IEA, 2018. International Energy Agency. World Energy Balances: Overview (2018 Edition), https://webstore.iea.org/world-energy-balances-2018-overview (27.1.2019)

Kim, M., Pettersen, J., Bullard, C. W., 2004. Fundamental process and system design issues in CO2 vapor compression systems. Progress. in Energy and Combustion Science 30(2), 119-174

Longo, G.A., 2010. Heat transfer and pressure drop during hydrocarbon refrigerant condensation inside a brazed plate heat exchanger. International Journal of Refrigeration 33(5), 944-953

Longo, G.A., 2012. Hydrocarbon Refrigerant Vaporization Inside a Brazed Plate Heat Exchanger. Journal of Heat Transfer 134(10), 101801 1-10

Longo, G.A., Mancin, S., Righetti, G., Zilio, C., 2015. A new model for refrigerant boiling inside Brazed Plate Heat Exchangers (BPHEs). International Journal of Heat and Mass Transfer 91, 114-149

Lorentzen, G., 1990. Trans-critical vapour compression cycle device. Patent WO/07683

Martin, H., 2013. Druckverlust und Wärmeübergang in Plattenwärmeübertragern. In: Verein Deutscher Ingenieure, VDI-Wärmeatlas, Springer Vieweg, Berlin, 1687-1693

Moisi, H., Rieberer, R., 2016. Erforderliche Sauggasüberhitzung bei einer R600-Hochtemperaturwärmepumpe – Nutzung der Motorabwärme. Proc. Deutscher Kälte- und Klimatechnischer Verein (DKV)-Tagung. Kassel, Germany, November 2016, paper II.2.15.

Moisi, H., Rieberer, R., Verdnik, M., Baumhakel, A., 2017. Entwicklung einer R600-Hochtemperatur-Wärmepumpe - Simulation und erste Messungen. Proc. Deutscher Kälte- und Klimatechnischer Verein (DKV)-Tagung. Bremen, Germany, November 2017, paper AA IV 08

Moisi, H., Rieberer, R., 2018. Experimental Analysis of a R600 High Temperature Heat Pump. Proc. 13th IIR Gustav Lorentzen Conference. Valencia, Spain, June 2018, paper 1223

Moisi, H., Rieberer, R., Baumhakel, A., 2018. "HotCycle" – Final Project Report (FFG-Nr.: 848892). Insitute of Thermal Engineering, Graz University of Technology, Graz

TLK-Thermo, 2018. TIL Suite v.3.6.0, TLK-Thermo GmbH, Braunschweig, Germany

UNEP, 2016. The Kigali amendment to the Montreal Protocol: HFC phase-down, ozonaction fact sheet. 8th Meeting of the Parties to the Montreal Protocol, Kigali, Rwanda, UNEP, 1-7

Viking, 2018. Viking Heat Engines AS. Heat Booster. Product Information. http://www.vikingheatengines.com/upl/files/142690 (5.4.2018)